FLUIDIZATION VIII

Proceedings of the
Eighth Engineering Foundation Conference
on Fluidization

May 14-19, 1995
Tours, France

Edited by

Jean-François Large and Claude Laguérie

Engineering Foundation
345 East 47th Street
New York, NY 10017

Library of Congress Catalog Card Number: 96-085044
ISBN 0-939204-54-1

SIMILARITY OF RADIAL PROFILES OF SOLID VOLUME FRACTION IN A CIRCULATING FLUIDIZED BED

BEAUD F., Electricité de France, Direction des Etudes et Recherches,
6, quai Watier, 78401 CHATOU CEDEX 01 (FRANCE)

LOUGE M., Sibley School of Mechanical and Aerospace Engineering,
Cornell University, Ithaca, NY 14853 (USA)

ABSTRACT

Fluid dynamic similarity with high-temperature CFB risers of varying diameter is achieved in a laboratory facility. For risers of moderate diameters, we establish that the radial profiles of local solid volume fraction are independent of riser size. This work complements the earlier study of Chang and Louge on the scale-up of axial pressure profiles. Unless the suspension is nearly collapsed, we observe also that these profiles, once made dimensionless with the average cross-sectional solid volume fraction, are self-similar.

Because measurements in industrial circulating fluidized beds (CFB) are challenging, small scale, generally cold, facilities are often used to produce design guidelines. To ensure that the data from these experimental units are relevant to CFB combustors, it is convenient to employ dimensional analysis and match the hydrodynamics of the cold facility to that of an industrial unit. However, because this analysis rests upon implicit assumptions on the physics of the flow, the scale-up rules derived from the analysis must be demonstrated experimentally.

Glicksman (1) first derived scaling relationships for bubbling beds. For CFBs, Louge (2) added the ratio of the particle-to-gas mass flow rates to Glicksman's dimensionless groups. Glicksman's dimensional analysis for CFBs (3) is identical to that of Chang and Louge (4,5), except that these authors incorporate the particle sphericity with the particle diameter in the relevant dimensionless groups. Using a semi-empirical model, Horio et al. (6) produced a different set of dimensionless numbers, which is primarily valid in the viscous limit of flow around a single particle. Finally, Glicksman et al. (7) recently developed a simplified set of scaling parameters for CFBs.

Several experimental verifications of these relationships have been carried out. Glicksman et al. (3) compared vertical voidage profiles and pressure fluctuations of a CFB combustor at the University of British Columbia and its quarter-scale cold model. They found good agreement but outlined effects of small geometric discrepancies and

of particle or wall surface properties. More recently, Westphalen and Glicksman (8) demonstrated Glicksman's scale-up rules using a 2.5MWth CFB combustor and its quarter-scale cold model. Glicksman et al. (7) successfully tested their simplified rules on similar hot and cold units. Horio et al. (6) and Ishii et Murakami (9) also reported good agreement with the performance of two laboratory-scale cold CFBs, using the similarity rules derived from Horio (6) in the viscous limit.

Using a single cold facility with the ability to recycle fluidization gas mixtures of adjustable density and viscosity, Chang and Louge (4,5) achieved fluid dynamic similarity with generic high-temperature CFB risers of 0.32, 0.46 and 1m diameter by suspending plastic, glass and steel powders in mixtures of helium and carbon dioxide. Because in the corresponding experiments with the three powders Chang and Louge matched all dimensionless groups except the particle-to-bed diameter ratio, they effectively observed the effects of scale-up on the global hydrodynamics of the flow. In combustors of moderate diameters, they found that vertical profiles of static pressure scale with the riser height and the material density of the particles, while pressure fluctuations scale with the particle diameter. In contrast, Chang and Louge found that risers of larger diameter exhibit an incipient choking characterized by larger vertical pressure gradients, a considerably denser bottom region, and more intense pressure fluctuations. While validating their dimensional approach, Chang and Louge thus provided insight on the evolution of the pressure profiles between small laboratory beds and larger industrial facilities.

The present paper focuses on moderate riser diameters through suspensions of plastic and glass powders. To the earlier results of Chang and Louge obtained in the same facility (4,5) it adds the effects of scale on the radial profiles of time-averaged local solid volume fraction. We begin with a brief synopsis of the dimensional analysis, the facility and its instruments. We elaborate on the calibration of the optical fiber probe used to measure local solid volume fraction and point out some of its shortcomings.

DIMENSIONAL ANALYSIS

From the equations of motion and boundary conditions for a system of fluidized particles (Anderson and Jackson, 10), Chang and Louge (4,5) obtain five dimensionless groups, which characterize the fluid dynamics of the riser along with the relative particle size distribution (PSD) and geometrical aspect ratios,

$$\mathrm{Fr} \equiv \frac{u}{\sqrt{gd\phi}}, \quad \mathrm{Ar} \equiv \frac{\rho_s \rho (d\phi)^3 g}{\mu^2}, \quad R \equiv \frac{\rho_s}{\rho}, \quad M \equiv \frac{G}{\rho u}, \quad L \equiv \frac{D}{d\phi}.$$

Here u and G are the superficial gas velocity and solid flux, respectively; ρ, μ, ρ_s, d, and ϕ are the density of the gas, its viscosity, the material density of the solids, their mean Sauter diameter and sphericity, respectively; g is the acceleration of gravity and D is the riser diameter. To observe the effects of scale-up alone, Chang and Louge match all groups except L between the cold bed and a generic coal combustor of diameter D_c operating with $\rho_s \approx 1500 \mathrm{kg/m^3}$, $\rho \approx 0.3 \mathrm{kg/m^3}$, $\mu \approx 4.6.10^{-5} \mathrm{kg/m.s}$ and $\phi d \approx 280 \mu\mathrm{m}$. As Table 1 indicates, they employ suspensions of plastic and glass in mixtures of helium and carbon dioxide to simulate the effects of changing L.

Table 1. Experimental Conditions.

He (%)	CO_2 (%)	ρ (kg/m^3)	$\mu \times 10^{-5}$ (kg/m.sec)	Powder	ρ_s (kg/m^3)	d (μm)	ϕd (μm)	D_c (m)	Ar (-)	R (-)	L (-)
92	8	0.30	2.0	Plastic grit	1440	234	162	0.34	45	4808	1215
79	21	0.52	1.9	Glass beads	2530	109	109	0.51	45	4905	1806

Making the static pressure profiles dimensionless with the product $\rho_s gH$, Chang and Louge (4,5) found that, over a wide range of operating conditions in Fr and M, the dimensionless pressure profiles $p^\dagger$ obtained with the glass and plastic powders coincide and thus are independent of L. For a given geometry and PSD,

$$p^\dagger \equiv \frac{\bar{p}-\bar{p}_{top}}{\rho_s g H} = \text{function}\left(\frac{z}{H}, Fr, M, Ar, R\right),$$

where z and H denote the distance from the gas distributor and the riser height, respectively.

Consequently, the vertical profiles of average cross-sectional voidage are also independent of L for moderate diameters,

$$(1-\bar{\varepsilon}) = \frac{\partial p^\dagger}{\partial(z/H)} = \text{function}\left(\frac{z}{H}, Fr, M, Ar, R\right).$$

Similarly, Chang and Louge found that the probability density function (PDF) of the dimensionless pressure fluctuations p' for the plastic and the glass powders is independent of L over a wide range of operating conditions,

$$\text{PDF}\left(p' \equiv \frac{p-\bar{p}}{\rho_s g d\phi}\right) = \text{function}\left(p', \frac{z}{H}, Fr, M, Ar, R\right)$$

Glicksman privately suggested that because $\rho_s g d\phi = \rho u^2 R/Fr^2$, the pressure fluctuations p' also scale with the kinetic energy density of the gas.

In an attempt to validate our dimensional analysis further, we now focus on the radial profiles of local, time-averaged solid volume fraction in the limit of moderate riser diameters.

APPARATUS

Chang and Louge (4,5) describe in detail the facility sketched in Fig. 1 and its operations. It is designed to prepare and recycle any mixture of helium and carbon dioxide.

Static pressure is measured using 25 taps mounted flush along the height of the riser. The taps are read in sequence with a scanning valve connected to a single pressure transducer.

We measure radial profiles of solid volume fraction with an optical fiber probe (MTI Fotonic 125R) consisting of a group of transmitting and receiving fibers of 0.55 N.A. randomly bundled inside an active diameter of 2.18mm and protected by a 30cm long stainless steel tube of 3.73mm diameter. The active diameter is several times larger than the mean particle size to avoid excessive uncertainties of the probe signal (11). The commercial amplifier connected to the probe detector provides a signal linear with light intensity.

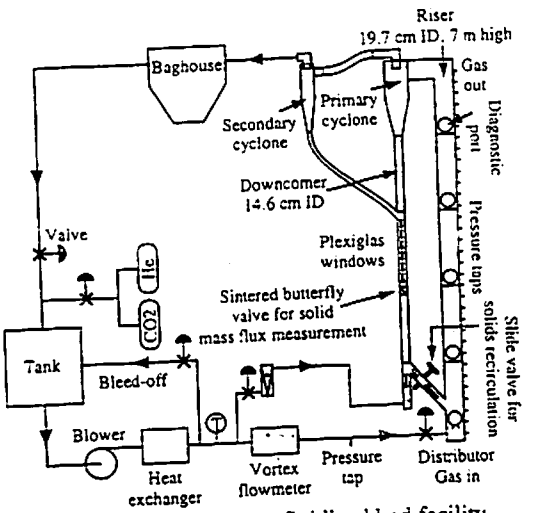

Fig. 1. The circulating fluidized bed facility.

OPTICAL PROBE CALIBRATION

We calibrate the optical probe against the quantitative wall capacitance probe of Acree Riley (12) in the manner described by Lischer and Louge (11). In this method, the optical probe is inserted flush with the wall through the grounded core of the capacitance probe. Once processed through a low-pass filter with a (-3dB) cutoff frequency of 90Hz and sampled at a rate of 180Hz, the simultaneous samples from the two probe signals are compared. For convenience, the signal from the capacitance probe is converted to a solid volume fraction using the model of Böttcher (Louge and Opie, 13). A point-by-point calibration graph is presented in Fig. 2. As suggested by Hartge et al. (14), the output voltage is fitted with the function $V = k(1-\varepsilon)^m$, where k and m are two adjustable parameters.

The calibration graphs usually exhibit considerable scatter for three main reasons. The first is associated with the relative lack of coincidence of the measurement volumes along the wall surface. This induces occasional time lags between events recorded by the two probes. Nevertheless, because cross-correlations of the signals failed to reveal any systematic time lag, we anticipate that the time-averaged acquisitions are unaffected by differences in the measurement volumes. The second cause for scatter is the dependence of the optical measurement volume on the particle volume fraction. Under dilute conditions, the optical probe is influenced by distant particles that do not affect the capacitance probe. The last cause of scatter arises from the greater sensitivity of the optical fiber to the placement, shape and physical aspect of the particles (11).

As the calibration data of Fig. 2 indicate, the response of the MTI fiber bundle is relatively disappointing. The slope of the voltage is moderate at high solid volume fractions, while at low volume fractions the output may be influenced by the far away structure of the flow. Our attempts to remedy the latter by adding a 2.5mm diameter plano-convex glass lens of 1.6mm focal length in front of the bundle failed to produce the expected improvement.

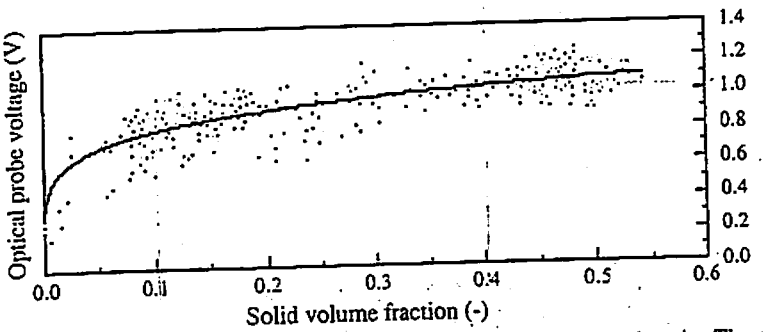

Fig. 2. Calibration plot for Fr = 170, M = 22, z/H = 0.163 with plastic grit. The solid line represents the exponential fit of the output voltage from the optical probe.

In the interior of the riser, the signal from the optical fiber is sampled at 180Hz. Samples are first converted to a solid volume fraction through the calibration fit before time-averaging over 30sec. A convenient test of the accuracy of the resulting average solid volume fractions is to compare these with the corresponding averages produced by the capacitance probe at the wall. Any systematic bias introduced by the calibration would likely produce significant discrepancies between the two time-averages. Because at the wall we consistently observe good agreement between these, the optical probe produces profiles of time-average particle volume fraction with sufficient sensitivity. However, it is clear that, unlike the capacitance probe, the optical fiber fails to yield accurate values of instantaneous volume fractions.

RESULTS

Experiments were conducted to simulate generic coal combustors of moderate diameter (L = 1215 and 1806) with superficial gas velocities and solid fluxes in the range $129 \le Fr \le 170$ and $8 \le M \le 21$. Figures 3a, 3b and 3c compare vertical voidage profiles inferred from the pressure measurements with plastic grit and glass beads. The coincidence of these profiles confirms the earlier conclusions of Chang and Louge that these are insensitive to the relative riser size $D/\phi d$ when the value of the latter is moderate (4).

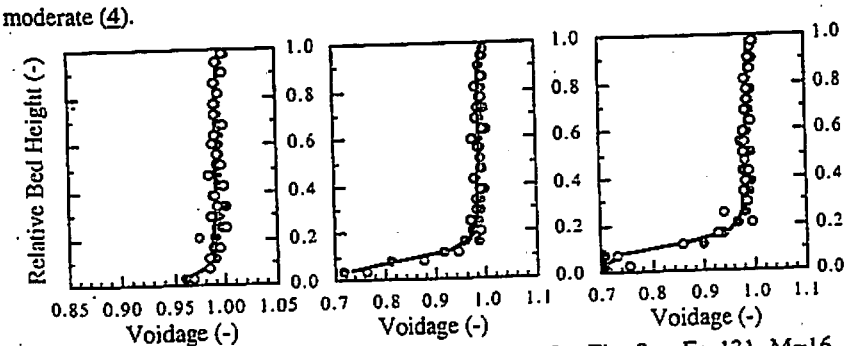

Fig. 3a. Fr≈129, M≈8. Fig. 3b. Fr≈129, M≈12. Fig. 3c. Fr≈131, M≈16. Open and solid symbols are L = 1215 and 1806, respectively. Solid lines are fits through the data.

The radial profiles of solid volume fraction are obtained by sliding the optical fiber through the center of the capacitance probe in 6.4mm increments up to a distance just beyond the axis of the riser. Figures 4, 5 and 6 compare radial profiles of local, time-averaged solid volume fraction obtained with plastic and glass powders. The radial distance r from the column center is made dimensionless with the riser diameter D. From these figures, we find that the radial profiles are similar within experimental uncertainties. Thus, like the vertical voidage profiles, the radial profiles of time-average particle volume fraction are independent of the dimensionless scale L of the riser for moderate riser diameters. Because the cross-sectional average solid volume fraction is the integral of the corresponding local values across the riser, our conclusions are consistent with those of Chang and Louge (4,5), at least in the range of moderate riser diameters considered in the present experiments ($1215 \leq L \leq 1806$). Although the optical sensor is not calibrated against the mean solid volume fraction inferred from the gas pressure transducer gradient, but instead against the measurements of the capacitance probe, the cross-sectional averaged solid fractions estimated from the direct integration of the radial profiles are in excellent agreement with those inferred from the gas pressure gradient (Fig. 5).

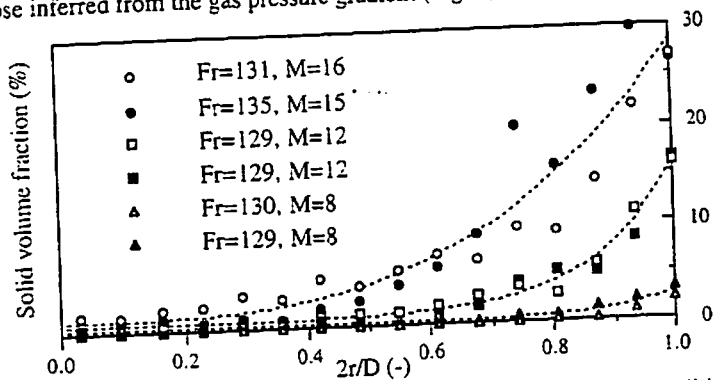

Fig. 4. Radial profiles of solid volume fraction for several analogous conditions at $z/H = 0.163$. The open and solid symbols are $L = 1215$ and 1806, respectively. The dotted lines are fits through the data.

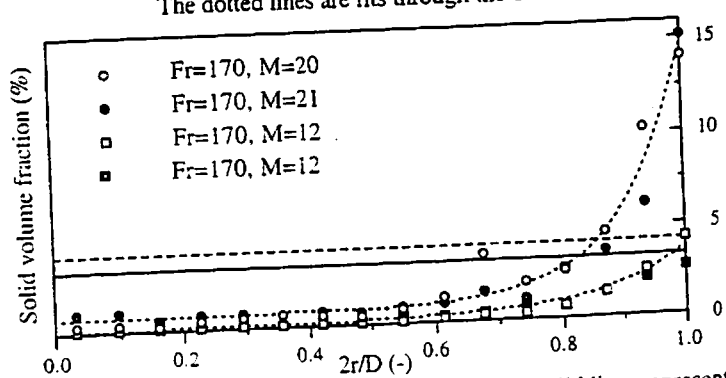

Fig. 5. Same caption as Fig. 4. The straight dashed and solid lines represent the cross-sectional average fractions inferred from the pressure transducers and from the optical probe, respectively, for $Fr \approx 170$ and $M \approx 20$.

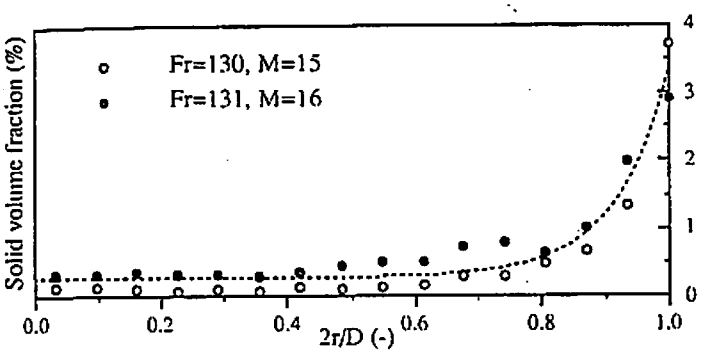

Fig. 6. Same caption as Fig. 4 except z/H = 0.522.

Finally, it is instructive to consider the "self-similarity" of the radial profiles of solid volume fraction. As Fig. 7 indicates, our data for either the glass and plastic powders show that these profiles, once made dimensionless with the cross-sectional average volume fraction, become independent of operating conditions, with one notable exception. We observe a significant departure from the self-similarity in the bottom region of a nearly collapsed riser suspension. As Fig. 3 illustrates, increasing the solid flux at given gas velocity causes the lower region to become denser and higher, as the suspension exhibits incipient collapse. For Fr ≈ 131 and M ≈ 16, the bottom region reaches the lower position of the optical probe at z/H = 0.163. In this region, the radial profile is markedly flatter than the self-similar profiles. Nevertheless, under the same conditions, the top riser region still exhibits self-similarity.

Other works have previously mentioned the existence of a self-similarity for both local solid fraction and solid flux profiles. Herb et al. (15) note that all profiles of solid volume fraction, once made dimensionless with the cross-sectional average volume fraction, are independent of the conditions. Chen and Chen's data (16) reveal a similar trend. Rhodes et al. (17) experimentally demonstrate that, at a given superficial gas velocity, all radial profiles of solid flux, once divided by the mean solid flux G, coincide provided the riser operates in the refluxing transport regime. These authors also quote results from other workers who observe a similar behavior for the reduced radial profiles of solid volume fraction. Lastly, Zhang et al. (18) empirically relate the local solid volume fraction to its cross-sectional average. This correlation does not quite satisfy the self-similarity of the radial profiles of solid volume fraction. The departure from self-similarity is nevertheless negligible in the core of the riser and is quite small close to the wall.

CONCLUSIONS

This study confirms that the dimensionless parameters Fr,Ar, R, M, L, PSD and H/D proposed by Chang and Louge (4) govern the distribution of local solid volume fraction in a circulating fluidized bed. For risers of moderate diameters, we find the voidage to be independent of unit size and the radial profiles of solid volume fraction to exhibit self-similarity in the upper, dilute region of the riser.

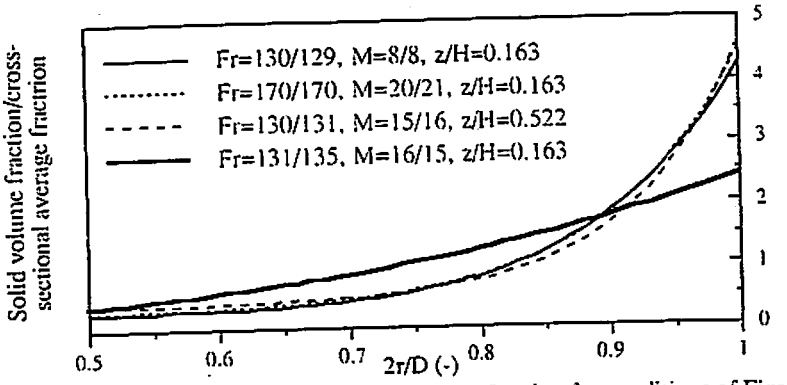

Fig. 7. Relative radial profiles of solid volume fraction for conditions of Figs. 4, 5 and 6. For clarity, the lines represent the best fits from these Figs.

ACKNOWLEDGEMENTS

This work, carried out at Cornell University, was sponsored by Electricité de France. The authors are grateful to Air Products & Chemicals for supplying all gases used in these experiments. There are also indebted to Edward P. Jordan for helping to assemble the optical fiber probe and to Stéphane Martin-Letellier for assisting with the experiments.

NOTATION

D	riser diameter [m]
H	riser height [m]
d	particle mean Sauter diameter [m]
u	superficial gas velocity [$m.s^{-1}$]
G	solid mass flux [$kg.m^{-2}.s^{-1}$]
p	gas pressure [Pa]
$\bar{p}$	time-averaged gas pressure [Pa]
$\bar{p}_{top}$	gas pressure at the top of the riser [Pa]
p^+	dimensionless gas pressure = $\frac{\bar{p}-\bar{p}_{top}}{\rho_s g H}$ [-]
p'	dimensionless gas pressure fluctuations = $\frac{p-\bar{p}}{\rho_s g d\phi}$ [-]
z	elevation with origin at the bed distributor [m]
r	distance from the center of the riser [m]
g	acceleration of gravity [$m.s^{-2}$]
Fr	Froude number = $\frac{u}{\sqrt{gd\phi}}$ [-]
Ar	Archimedes number = $\frac{\rho_s \rho (d\phi)^3 g}{\mu^2}$ [-]
R	density ratio = $\frac{\rho_s}{\rho}$ [-]

M	solid loading $= \frac{G}{\rho u}$ [-]
L	diameter ratio $= \frac{D}{d\phi}$ [-]
V	optical probe output voltage [V]
k	pre-exponential factor of the optical probe calibration [V]
m	exponent of the optical probe calibration [-]
ϕ	particle sphericity [-]
ρ	gas density [$kg.m^{-3}$]
ρ_s	solid density [$kg.m^{-3}$]
μ	gas viscosity [$kg.m^{-1}.s^{-1}$]
ϵ	local voidage [-]
$\bar{\epsilon}$	average cross-sectional voidage [-]
c	subscript indicating a generic coal combustor

REFERENCES

1. Glicksman, L.R., Chemical Engineering Science, Vol. 39, No. 9, pp. 1373-1379 (1984)
2. Louge, M.Y., Proceedings of the Ninth International Conference on FBC, Boston, MA, ASME, in J. Mustonen (ed.), pp. 1193-1197 (1987)
3. Glicksman, L.R., Westphalen, D., Brereton, C. and J. Grace, Preprints of the Third International Conference on CFB, Nagoya, Japan (1990)
4. Chang, H. and M. Louge, Powder Technology, 70, pp. 259-270 (1992)
5. Chang, H., Ph.D. Thesis, Cornell University, Ithaca, NY (1991)
6. Horio, M., Ishii, H., Kobukai, Y. and N. Yamanishi, Journal of Chemical Engineering of Japan, vol. 22, pp. 587-592 (1989)
7. Glicksman, L.R., Hyre, M. and K. Woloshun, Powder Technology, 77, pp. 177-199 (1993)
8. Westphalen, D. and L. Glicksman, Preprints of the Fourth International Conference on CFB, Somerset, PA (1993)
9. Ishii, H. and I. Murakami, Preprints of the Third International Conference on CFB, Nagoya, Japan (1990)
10. Anderson, T.B. and R. Jackson, Ind. Eng. Chem. Fundamentals, Vol. 6, No. 4, pp. 527-539 (1967)
11. Lischer, D.J. and M. Louge, Applied Optics, Vol. 31, No. 24, pp. 5106-5113 (1992)
12. Acree Riley, C. and M. Louge, Particulate Science & Tech., 7, pp. 52-59 (1989)
13. Louge, M. and M. Opie, Powder Technology, 62, pp. 85-94 (1990)
14. Hartge, E.U., Rensner, D. and J. Werther, Chem. Ing. Tech., 61, pp. 744-745 (1989)
15. Herb, B., Tuzla, K. and J. Chen, in Fluidization VI, ed. J.R. Grace, L.W. Shemilt and M. Bergougnou, Engineering Foundation, New York, pp. 65-72 (1989)
16. Chen, C.C. and C.L. Chen, Chemical Engineering Science, Vol. 47, No. 5, pp. 1017-1025 (1992)
17. Rhodes, M.J., Wang, X.S., Cheng, H. and T. Hirama, Chemical Engineering Science, Vol. 47, No. 7, pp. 1635-1643 (1992)
18. Zhang, W., Tung, Y and F. Johnsson, Chemical Engineering Science, Vol. 46, No. 12, pp. 3045-3052 (1991)